# Implications of the coffee-ring effect on virus infectivity

*Qishen Huang, Wei Wang, Peter J. Vikesland**

Civil and Environmental Engineering and Institute of Critical Technology and Applied Science (ICTAS) Sustainable Nanotechnology, Virginia Tech, Blacksburg, Virginia, 24061, USA

Keywords: virus infectivity, coffee-ring effect, sessile droplet.

*Corresponding author e-mail: pvikes@vt.edu

**Abstract**

The factors contributing to the survival of enveloped viruses (e.g., influenza and SARS-CoV-2) on fomite surfaces are of societal interest. The bacteriophage Phi6 is an enveloped viral surrogate commonly used to study viability. To investigate how viability changes during the evaporation of droplets on polypropylene, we conducted experiments using a fixed initial Phi6 concentration while systematically varying the culture concentration and composition (by amendment with 2% FBS, 0.08%wt BSA, or 0.5%wt SDS). The results were consistent with the well-founded RH effect on virus viability; however, the measured viability change was greater than that previously reported for droplets containing either inorganic salts or proteins alone, and the protein effects diverged in 1×Dulbecco's Modified Eagle's Medium (DMEM). We attribute this discrepancy to changes in virus distribution during droplet evaporation that arise due to the variable solute drying patterns (i.e., the 'coffee-ring' effect) that are a function of droplet biochemical composition. To test this hypothesis, we used surface-enhanced Raman spectroscopy (SERS) imaging and three types of gold nanoparticles (pH nanoprobe, positively charged (AuNPs(+)), and negatively charged (AuNPs(-))) as physical surrogates for Phi6 and determined that lower DMEM concentrations as well as lower protein concentrations suppressed the coffee-ring effect. This result was observed irrespective of particle surface charge. The trends in the coffee-ring effect correlate well with the measured changes in virus infectivity. The correlation suggests that conditions resulting in more concentrated coffee-rings provide protective effects against inactivation when viruses and proteins aggregate.

## Introduction

The SARS-CoV-2 virus responsible for the COVID-19 pandemic is transmitted by aerosols and droplets produced when an infected individual speaks, coughs, sneezes, sings, or breathes.[1–8] Aerosolized droplets potentially collect on surfaces (i.e., fomites) and may remain infectious.[9–13] Human exhalate contains respiratory fluids that serve as the carrier of respiratory viruses such as SARS-CoV-2 and influenza virus.[14,15] These respiratory fluids (e.g., saliva, lung fluid, etc.) have complicated chemical and biochemical compositions that reflect the location and processes responsible for exhalate production.[14,16] Important fluid constituents include surfactants, fatty acids, and proteins.[16] Proteins, in particular, are thought to provide protective effects that enhance virus viability.[4]

Infective viruses persist on surfaces for periods ranging from hours-to-days depending on the environmental conditions (e.g., temperature and relative humidity (RH), surface material, and viral suspension media).[12,13,17,18] Prior studies have shown a consistent decline in SARS-CoV-2 half-life with increased temperature (from around a days to hours with a ≈10 °C increase in temperature) under moderate RH (20 – 60%) conditions; more extreme RH conditions better preserve the virus.[19,20] More generally, surface material and suspension media are known to affect the persistence of enveloped viruses, with half-lives varying from tens of hours on plastic surfaces to 1-2 hours or even less on metal surfaces.[10,12,21,22] Both surface material identity and suspension media dictate the drying behavior of droplets on surfaces as they collectively define the surface tension between the surface, the droplet, and the surrounding air.[23] Improved characterization of droplet evaporation on surfaces is needed to improve interpretation of virus longevity data and to advance infection control in health care facilities, households, and communities.

53 When a sessile droplet (e.g., a static droplet on a surface) dries, the non-volatile components
54 within the droplet often deposit at the water-surface contact line. This phenomenon, known as
55 the 'coffee-ring effect',[23,24] reflects the balance between capillary and Marangoni flows in a
56 drying droplet.[25] Capillary flows deposit particles at the water-surface contact line whereas
57 Marangoni flows transport particles from the periphery to the center.[26] These different convection
58 and deposition processes dominate at different evaporation stages and collectively give rise to the
59 final deposition pattern.[27,28] Past studies have shown the coffee-ring effect is affected by surface
60 hydrophobicity,[29] pH,[30] droplet chemical composition[31] as well as particle morphology.[32] Within
61 industry, control of the coffee-ring effect can be very important during material manufacturing
62 processes.[23] Of relevance to the present work is the recognition that the coffee-ring effect
63 enhances performance of surface-enhanced Raman spectroscopy (SERS) substrates through
64 aggregation of gold nanoparticles (AuNPs) and analytes.[33,34]
65 Aggregation can provide a 2 to 10× increase in viral resistance to disinfection, thus enhancing
66 virus survival and longevity.[35,36] We hypothesized that the relative magnitude of the coffee-ring
67 effect, which alters the spatial deposition of viruses on surfaces, can impact viability. To test this
68 hypothesis, we conducted studies examining how coffee-ring formation impacted the viability of
69 the bacteriophage Phi6 under various RH and droplet compositions. Phi6 is an enveloped virus
70 often used as a surrogate.[37,38] SERS imaging can be used to determine the spatial distribution of
71 nanoscale target analytes within droplets.[39,40] Unfortunately, direct detection and imaging of
72 viruses within a biomolecule laden matrix by SERS or any other light microscopy based
73 technique is extremely challenging. We therefore used AuNPs with similar geometrical shape,
74 size, and surface charge as physical viral surrogates to determine their spatial distribution during
75 droplet evaporation.[41] Past studies examining viral transport[42] and surface attachment[43] have

76 shown that appropriately charged and sized AuNPs are useful viral surrogates. To the best of our
77 knowledge, this is the first study relating virus infectivity to drying-induced aggregation within
78 sessile droplets.

79 **Experimental**

80 **Chemicals and Virus.** All chemicals were used directly as purchased. Dulbecco's Modified
81 Eagle's Medium (DMEM 1×, MiliporeSigma D6546) with high glucose (4500 mg/L) and
82 supplementations (1% L-glutamine, 1% penicillin-streptomycin (Pen/Strep), and 2% fetal bovine
83 serum (FBS)) was kindly provided by Dr. Vincent J. Munster of the U.S. National Institutes of
84 Health. The detailed DMEM composition is listed in Table S1. Phi6 virus was propagated in the
85 bacterial host *Pseudomonas syringae* (suspended in Luria-Bertani broth (LB) with 0.75%
86 autoclaved agar) on LB agar plates and cultured at 25 °C for 24 h. Propagated Phi6 was purified
87 by filtration through a 0.22 $\mu$m cellulose acetate filter. The propagated Phi6 was resuspended into
88 DMEM after ultra-centrifugation (59,100 ×g, 2 hrs) and stored in a 4 °C freezer as stock culture.
89 The titer of the stock culture was $\approx 10^9$ plaque forming units (PFU/mL). The initial Phi6 titers of
90 all sessile droplets in this study were $\approx 10^6$ PFU/mL, a 1000× dilution from the stock culture, to
91 minimize interference from the original culture medium (e.g., protein and salt residues from LB).
92 **AuNP Synthesis.** Three different AuNPs with distinct sizes and surface charges were
93 synthesized: positively charged (AuNPs(+)), negatively charged (AuNPs(-)), and a pH
94 nanoprobe. Synthesis of AuNPs(+) followed the method of Li et al[44] with modification of the
95 volumes of $NaBH_4$ (0.2 mL, 100 mM), $HAuCl_4$ (2 mL, 1 mM), and cetyl trimethyl ammonium
96 bromide (CTAB, 2 mL, 10 mM) to generate larger sized AuNPs(+). The suspension was stirred
97 15 min and the AuNPs(+) were centrifugally washed (4900 ×g, 15 min). AuNPs(-) were
98 synthesized by a seed-mediated growth method adapted from Yuan et al.[45] AuNP seeds were

99 produced by refluxing 15 mL of 1% $Na_3Citrate{\cdot}2H_2O$ with 100 mL of boiling 1 mM
100 $HAuCl_4{\cdot}3H_2O$ for 15 mins and then filtered through a 0.22 $\mu$m nitrocellulose filter after cooling.
101 Ascorbic acid (50 $\mu$L, 100 mM) was added to the synthesized AuNP seeds (100 $\mu$L) and 10 mL
102 solution containing 0.25 mM $HAuCl_4{\cdot}3H_2O$ and 1 mM HCl to initiate Au(III) reduction. The
103 suspension was mixed 30 s prior to centrifugation (4900 ×g, 15 min). pH nanoprobe synthesis is
104 described elsewhere.[40,46,47] The pH nanoprobes were 4-mercaptobenzoic acid (4-MBA)
105 functionalized AuNPs with a polyethylene glycol thiol (m-PEG-SH, 5 kDa) protective layer.
106 **Characterization of AuNPs and Phi6.** Synthesized AuNPs and propagated Phi6 were dispersed
107 in DI water and characterized by dynamic light scattering (DLS; Malvern Zetasizer Nano-ZS
108 3600) for Z-average sizes and electrophoretic mobilities ($U_E$, $m^2 \cdot V^{-1} \cdot S^{-1}$), and by scanning
109 electron microscope (SEM) for the approximate relative size (Figure S1). The measured sizes
110 and electrophoretic mobilities of the AuNPs and Phi6 are listed in Table 1.
111 *Table 1. Sizes and electrophoretic mobilities of Phi6 and nanoparticles measured by DLS and SEM.*

| Sample Type | Phi6 | pH nanoprobe | AuNPs(+) | AuNPs(-) |
|---|---|---|---|---|
| **Z-average (nm)** | 88.1 ± 4.0 | 111.9 ± 9.2 | 56.2 ± 15.4 | 41.0 ± 0.9 |
| **Size - SEM (nm)** | 102.6 ± 21.2 | 81.3 ± 51.2 | 55.4 ± 20.4 | 46.6 ± 10.3 |
| **$U_E$ ($m^2 \cdot V^{-1} \cdot S^{-1}$)** | -0.75 ± 0.08 | -1.01 ± 0.07 | +4.19 ± 0.02 | -2.14 ± 0.24 |

112 **Evaporation of sessile droplets.** The evaporation of 5 $\mu$L sessile droplets on polypropylene
113 (ePlastics, reference PRONAT.030X24X47S/M) was quantified inside an Electro-Tech Systems
114 5518 environmental chamber. Polypropylene is a commonly used commercial surface which was
115 investigated by Morris et al to study SARS-CoV-2 inactivation.[20] In this study, the smooth side of
116 the polypropylene substrate was consistently used and SEM images of the smooth surface can be
117 found in Figure S2. Experiments were conducted at 25 °C under three RH conditions (25%,
118 50%, and 75%) using a series of DMEM dilutions (1× to 0.001×). Substrates was rinsed 3× with
119 1M sulfuric acid and ethanol before the experiments. Droplet mass was measured inside the

environmental chamber by placing the substrate onto a microbalance (Sartorius MSE3.6P-000-DM) and then pipetting a droplet directly on the substrate. The change in droplet mass was digitally recorded every minute. The balance chamber was left half-open to maintain air circulation during the measurements. This airflow decreased balance accuracy to ≈ 0.01 mg. As justified in the SI, we calculated the evaporation rate of each droplet using linear-regression due to a negligible contact angle.[48,49] Evaporation rates determined using contact angle were estimated from droplet photos using ImageJ and the values were consistent with those determined gravimetrically (Figure S3). Final droplet residues were observed using an EVOS-FL2 microscope.

**Phi6 infectivity.** Plaque assays, following the procedure of previous studies from Dr. Marr group[7], were performed to quantify Phi6 in PFU/mL for stock culture, control (bulk samples), and experimental 5 $\mu$L droplets. Droplet residues were collected after complete evaporation (1 h for RH 25 & 50%, 2h for RH 75%) by pipetting the original DMEM (50 $\mu$L in total) onto the substrate and rinsing 20×. The relative infectious ratio for Phi6 = $\frac{C_t}{C_0}$, where $C_0$ and $C_t$ are the Phi6 concentration before and after evaporation. Phi6 infectivity is reflected by the $\log_{10}$ decay ($-\log_{10}(\frac{C_t}{C_0})$): a lower $\log_{10}$ decay indicates less change in Phi6 infectivity. The Phi6 infectivity change was observed under various droplet dilution chemistries: 1) supplemented DMEM (Table S1); 2) DMEM with no supplementations; 3) DMEM with 2% FBS (≈ 800 $\mu$g/mL protein); 4) DMEM with bovine serum albumin (BSA, 0.08%wt, ≈ 800 $\mu$g/mL protein).

**The coffee-ring effect in sessile droplets.** Sessile droplets (5 $\mu$L) containing AuNPs were monitored via SERS to quantify the coffee-ring effect. A home-made chamber compatible with our WITec Alpha 500R Raman controlled RH during droplet evaporation. Saturated potassium acetate and NaCl were used to maintain RH 25% and 75%, and the lab RH during the summer

was stable at ~50%. RH within the chamber was monitored before and after each experiment. The measured RH values were 25.6 ± 0.1%, 50.8 ± 0.4%, and 74.5 ± 1.3%, respectively. SERS maps of droplets were collected every 10 min at 25 and 50% RH and every 20 min at 75% RH. SERS maps of droplets were collected every 10 min at 25 and 50% RH and every 20 min at 75% RH using a 10× objective and a 3 mW 785 nm laser. Each SERS map consisted of 50 × 50 points that covered a droplet. SERS maps representing the AuNP spatial distribution were generated based upon the intensity of the pseudo-peak at ≈ 80 $cm^{-1}$. This pseudo-peak reflects the density of SERS hot-spots that formed due to AuNP aggregation.[50]

To succinctly describe temporal changes in the coffee-ring effect, we define the coffee ring coefficient (CRC). The CRC reflects the relative proportion of AuNPs that reside near the edge (i.e., a spatial distance within 20% of the initial wet droplet radius) of a dried droplet. Details about the CRC derivation can be found in the SI. If the AuNPs are homogeneously distributed across the droplet residue then CRC ≈ 0.36. As the magnitude of the coffee-ring effect increases the CRC approaches 1.

**The pH of droplets.** Droplet pH was calculated based upon SERS maps of droplets that contained pH nanoprobes.[40,46] In brief, the Raman spectrum of 4-MBA functionalized AuNPs has a pH-insensitive peak at 1080 $cm^{-1}$ and a pH-sensitive ($-COO^-$) peak at 1410 $cm^{-1}$. Ambient pH in the nanoprobe vicinity is estimated using the ratio of the peak intensities ($I_{1410}/I_{1080}$). The reported pH values reflect the average of the 250 most intense spectra for a given droplet.

## Results and Discussion

**Infectivity of Phi6 in DMEM droplets under different RH.** We incubated droplets containing $10^6$ PFU/mL of Phi6 in the presence of a range of DMEM concentrations (1× to 0.001×) at 25%, 50%, and 75% RH. The three selected RH values reflect typical RH for winter indoor (25%),

summer indoor (50%), and humid summer outdoor (75%) in the U.S. state of Virginia. The $\log_{10}$ decay of Phi6 was consistently lowest at RH 75% and highest at RH 25%, a result consistent with previous studies.[4,7,37] We note that the droplets were incubated for two hours at 75% RH to ensure complete droplet evaporation whereas droplets evaporated within an hour at 25 & 50% RH. At 75% RH, complete evaporation was determined as the time when the droplet mass plateaued at ≈100 mins (Figure S3) leaving a viscous droplet residue. The potential effects of changes in incubation time were evaluated to relate virus viability at 75% RH with that at 25 and 50% RH. We evaluated Phi6 decay at 1 h for 75% RH by measuring the virus infectivity change and by estimating Phi6 infectivity change assuming exponential decay.[19,51,52] Both observed and calculated Phi6 $\log_{10}$ decay at 1 h for 75% RH was comparable or slightly higher than the observed log decay at 50% for all DMEM concentrations (Figure S5). This indicates that additional inactivation, which might be related to the droplet drying patterns, happened between 1h and complete droplet evaporation at 75% RH. The same effect occurs at other RH values as well. The RH effect observed herein in which we consistently observe greater virus decay at higher RH agrees with prior studies over the same RH range,[37] thus validating our experimental procedures. For all RH values, we observed a decrease in Phi6 $\log_{10}$ decay at higher DMEM concentrations – indicating less decay in Phi6 infectivity and illustrating the protective effect of DMEM (Figure 1a). In the following parts of this study, we investigated how droplet composition affects evaporation rate, acidity, and the droplet drying pattern during evaporation, and then determined which parameters resulted in the greater protective effect.

**Evaporation rate and pH of sessile droplets.** The evaporation of sessile droplets is often described in terms of two modes: pinned contact line mode and constant contact angle mode with a receding contact line.[53–56] Droplet evaporation in this study followed the pinned contact line

189 mode except for a short period towards the end of evaporation which is reflected by the droplet
190 mass change shown in Figure S3 and the correlated change in CRC value depicted in Figure S5.
191 This result corroborates previous studies on sessile droplets containing both protein and salts.[57,58]
192 The evaporation rate of droplets containing only DMEM, DMEM with pH nanoprobes, DMEM
193 with Phi6, and DMEM with both pH nanoprobes and Phi6 was examined at RH 25% and 50%
194 (Figure S6). No quantifiable difference in evaporation rate was observed across these droplet
195 compositions thus indicating no effect of Phi6 or AuNP addition. Figure 1c shows the
196 evaporation rates for Phi6 containing droplets with different DMEM concentrations at the three
197 RH values. For any given RH, similar evaporation rates were observed across all DMEM
198 concentrations. Droplets evaporated most rapidly at RH 25% and slowest at RH 75%. The
199 measured evaporation rate directly reflects evaporation time since differences between the final
200 droplet masses for each RH and DMEM combination were negligible (~0.1mg, Figure S3).
201 Droplet pH might evolve during evaporation due to the changing concentration of
202 dissolved components.[52,59] We evaluated droplet pH over the course of droplet evaporation and
203 observed stable pH values (≈ 8) for all experimental conditions (Figure 1d). We attribute the
204 stable pH values to the buffer capacity provided by DMEM. The measured pH is closely
205 correlated with the ion distribution inside the droplets at the point of drying,[60] thus indicating the
206 relative ratios of the chemical species were consistent during droplet evaporation. The stable
207 evaporation rate and mean pH measured for different conditions indicates that neither of these
208 parameters differentially impacts virus viability under our test conditions.
209 **The effect of droplet composition on Phi6 infectivity.** We varied the composition and
210 concentration of DMEM droplets by adding additional proteins and surfactants to investigate the
211 effect of such additions on droplet virus infectivity. Prior work examined Phi6 decay in sessile

212 droplets using the same protocol. In that study, Lin et al observed an increase in virus
213 inactivation when the cumulative dose of NaCl increased and interpreted this result in terms of
214 CT (C = concentration, T = time of contact).[7,38] The major inorganic salts in DMEM are NaCl
215 (=6.4 g/L) and $NaHCO_3$ (=3.7 g/L). In our study (Figure 1a & 1b), at a given RH, lower initial
216 DMEM and thus lower salt concentrations resulted in greater loss of virus infectivity in both
217 supplemented and non-supplemented DMEM droplets. Such a relation contrasts with the effect
218 of salts on virus infectivity observed by Lin et al. and thus changes in NaCl do not account for
219 our findings.
220 We also investigated the effect of additional proteins on virus infectivity (Figure 1b). Droplets
221 with 2% FBS amendment (cyan line in Figure 1b) showed a consistent protein protective effect
222 regardless of the DMEM concentration. In droplets with 0.08% BSA (green line in Figure 1b) the
223 0.01× and 0.1× DMEM solutions exhibited protective effects; however, significantly greater
224 virus inactivation (~1 $\log_{10}$ unit higher) was observed in 1×DMEM and 0.08% BSA droplets
225 relative to 1×DMEM with 2% FBS thus suggesting a more complicated role of BSA alone on
226 Phi6 viability. The protective effects of proteins on Phi6 within suspended aerosols in a rotating
227 drum were quantified previously by Kormuth et al.[4] In that study, for RH between 55-75%, the
228 $\log_{10}$ decay of Phi6 declined ~1-2 when aerosolized in the presence of a human bronchial
229 epithelial (HBE) cell wash protein source (100-500 $\mu$g/mL). No apparent protective effect was
230 observed at either 23 or 30% RH. In this study, DMEM was supplemented with FBS protein and
231 protective effects were observed at 25% RH for high DMEM concentrations (~1 $\log_{10}$ unit less
232 decay). At 50% RH, the $\log_{10}$ decay for the 0.5× DMEM dilution, which has a comparable
233 protein concentration to that of Kormuth et al., was 2.4-$\log_{10}$ units lower than that for the 0.001×
234 dilution of DMEM. These results collectively show that changes in solution composition beyond

that of the protein alone impact Phi6 infectivity when sessile droplets dry. To further investigate this effect, we examined how different droplet composition and DMEM concentrations altered the droplet drying patterns and quantified the magnitude of the coffee-ring effect.

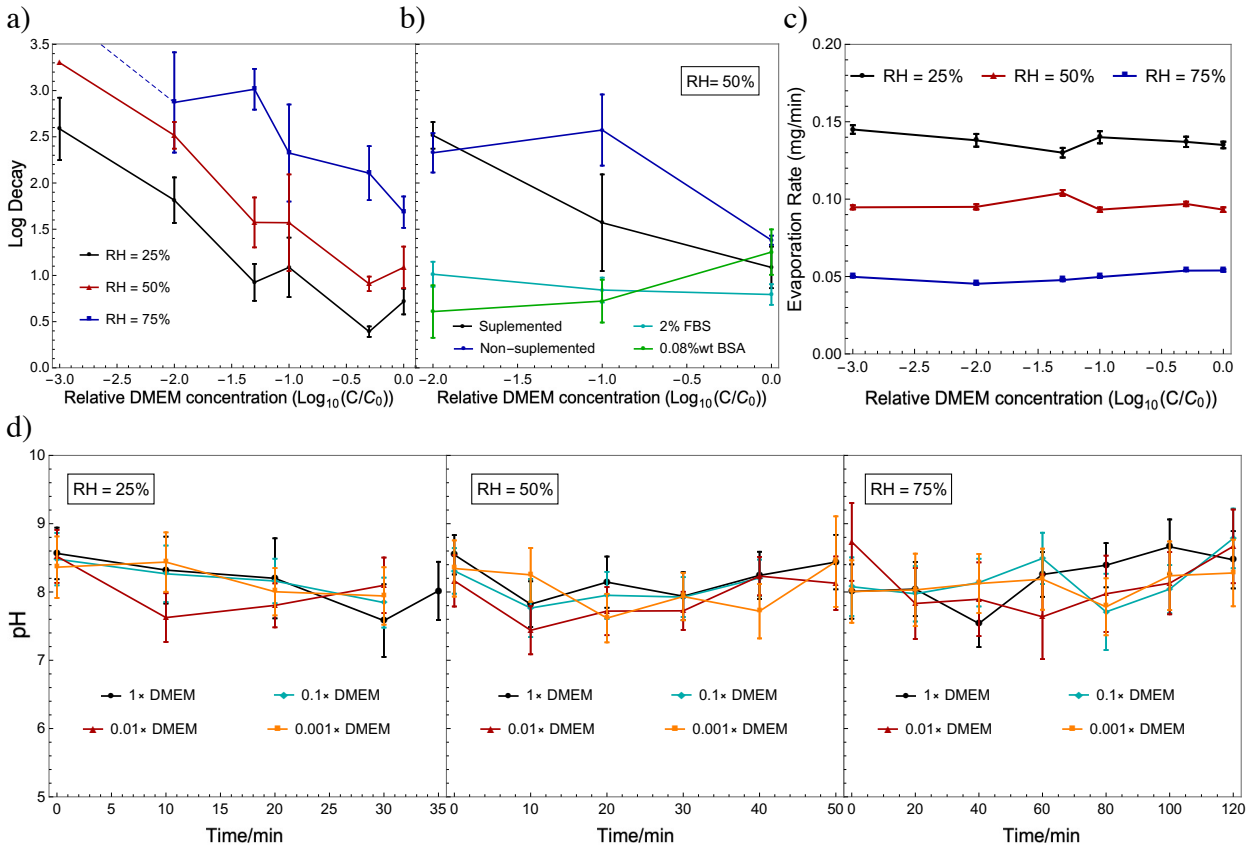


*Figure 1. a) $Log_{10}$ decay in virus infectivity as a function of RH and DMEM concentration. Each data point represents the average of triplicate experiments measured after complete evaporation of droplets. The error bar is the standard deviation from triplicates. The value 0 on the x-axis is equivalent to 1× DMEM, and the lower x-axis value refers to lower DMEM concentrations. b) The $Log_{10}$ decay of Ph6 after complete droplet evaporation at 50% RH. The droplet composition varied from dilutions of stock DMEM (supplemented with 2% FBS initially), dilutions of DMEM with no supplementation, and dilutions of DMEM with constant amount of two proteins, FBS and BSA. c) Evaporation rate of droplets at different DMEM concentration and RH. The lower x-axis represents the relative DMEM concentration in log scale, $C_0$ in the x-axis refers to the composition of stock DMEM (1×, Table S2). d) The droplet pH characterized by pH nanoprobe as a function of time during droplet evaporation for all DMEM concentrations and all three RH conditions.*

**The drying patterns of DMEM droplets.** Microscopic images of droplet residues for similar compositions consistently showed similar patterns. Droplet residues of supplemented DMEM + Phi6 are presented in Figure 2a. Images of droplet residues for other droplet compositions are

included in Figure 2b. Overall, droplet residues with higher initial protein concentrations exhibited an easily visible contact line whereas droplets with higher DMEM concentration are characterized by crystal structures within the interior of the droplet residues. Such inner crystal structures were not observed for low DMEM concentrations (< 0.01×, Figure 2a & 2b). The presence of a surfactant (0.5%wt SDS) suppressed formation of the inner crystal structures, but retained the contact line when the protein concentration was high (Figure S7). The SDS concentration investigated in this study was lower than the critical micelle concentration (CMC); similar uniform suppression of the coffee-ring effect was observed for SDS at concentrations lower than the CMC.[61] These microscopic photos are consistent with previously reported findings that the formation of the contact line is driven by protein concentration, whereas crystal structure development is driven by inorganic salts.[57,58] SEM images collected near the edge of the droplet residues suggest greater accumulation of droplet components in 1×DMEM droplet residues relative to more dilute DMEM suspensions (Figure S8). Importantly, the dendritic crystal structures formed within the 1× DMEM residues differ from the cuboidal crystals produced in droplets containing only NaCl (e.g., 0.1 M [equivalent to the concentration in 1× DMEM] in Figure 2c, and other concentrations in Figure S9). These differences reflect the combined effect of proteins and salts on dendritic crystallization.[62,63] Recent studies observed similar crystal structures in droplets of respiratory fluid surrogates on different substrates.[41,64] Even though proteins initiate coffee-ring formation, they may still deposit when salt crystals develop within the interior of the droplet residue. Similarly, inorganic salts may crystalize within the coffee-ring.[65]

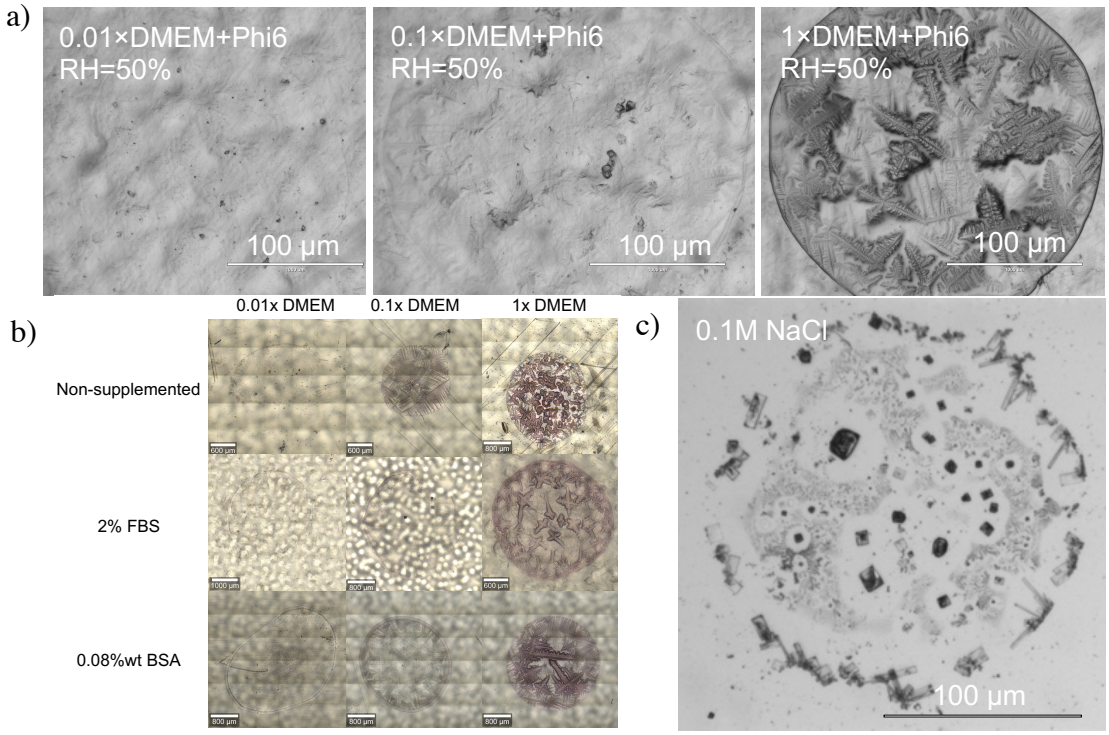


*Figure 2. a) Microscopic images of DMEM + Phi6 droplets after evaporation under 50% RH. b) Microscopic images of droplet residues for various droplet compositions: row 1) non-supplemented; row 2) fixed 2% FBS; row 3) fixed 0.08%wt BSA. c) Microscopic image of 0.1 M NaCl droplet residue. This NaCl concentration is similar to that in 1× DMEM.*

**AuNPs as surrogates for Phi6.** The observations obtained from the optical microscopic images are qualitative and it is not possible to visualize nanometer particles, such as Phi6; therefore, we used three types of AuNPs as nanoscale surrogates for Phi6 and employed SERS imaging to determine their spatial arrangements. Colloid deposition within a drying droplet can be affected by droplet surface tension and colloid concentration.[66,67] Previous modeling approaches of virus transport and attachment in subsurfaces as well as porous media have been following the theories developed for colloids (e.g. DLVO theory, extended DLVO theory) for decades.[42,43] The DLVO theory, which depict colloid stability, relied highly on the surface potential of colloids, and is the theoretical foundation for us to use AuNPs as spatial surrogate for Phi6. Moreover, in this study the small degree of variance in the initial contact angles (Table S2) for all droplets indicated that addition of Phi6 or the AuNPs did not alter the surface tension due to their relatively low

concentrations (Phi6 ≈$10^6$ PFU/mL, AuNPs ≈$10^8$ NPs/mL). Initial contact angles were measured for each polypropylene substrate and the small standard deviation (< 5°) showed the consistent surface properties of the substrates.

Using our SERS maps and a binary filter, we calculated the CRC as a function of time to evaluate the magnitude of the coffee-ring effect (Figure 3a & 3b). Note that the CRC evaluated from SERS maps directly reflects the relative coffee-ring effect of AuNPs and provides an indication of the Phi6 distribution due to their similar size and surface charge. Further investigation is needed to generalize how the CRC values reflect the distribution of all components in droplets. In general, for AuNPs, they were homogeneously distributed initially (CRC ≈ 0.3) and then exhibited variable accumulation patterns towards the end of evaporation. For all RH values, the CRC value for the 1× DMEM droplets increased significantly near the end of droplet evaporation. Figure 3b shows how the CRC values change over time for three types of AuNPs. Although there is variability in the CRC values across the different conditions, similar trends were observed for all AuNPs at RH 50% as well as for the pH nanoprobes at the other RH values (Figure S10). We calculated the CRC of initially supplemented DMEM droplets at the conclusion of droplet drying and report it in Figure 3c. This value reflects the final dried state for a given droplet. We observed a systematic decrease in the CRC with a decrease in the DMEM concentration thus suggesting suppression of the coffee-ring effect. The change in DMEM concentration alters the relative importance of surface tension gradient induced capillary flow relative to concentration gradient induced Marangoni flow and thus alters the final CRC.[25,68,69] As indicated in Table 1, the AuNPs had diameters ranging from 41 to 112 nm and electrophoretic mobility values varying from -1.01 to +4.19 $m^2 \cdot V^{-1} \cdot S^{-1}$. This range bounds the measured size (88.1 nm) and electrophoretic mobility (-0.75 $m^2 \cdot V^{-1} \cdot S^{-1}$) of Phi6. The similar trends

observed for AuNPs(+), AuNPs(-), and the pH nanoprobes suggest that deposition of colloids with sizes and surface charges within the range involved in this study should be similar during evaporation. Accordingly, the AuNPs, especially the pH nanoprobes, which have the closest size, charge, and most similar surface characteristics can be regarded as physical surrogates for Phi6.

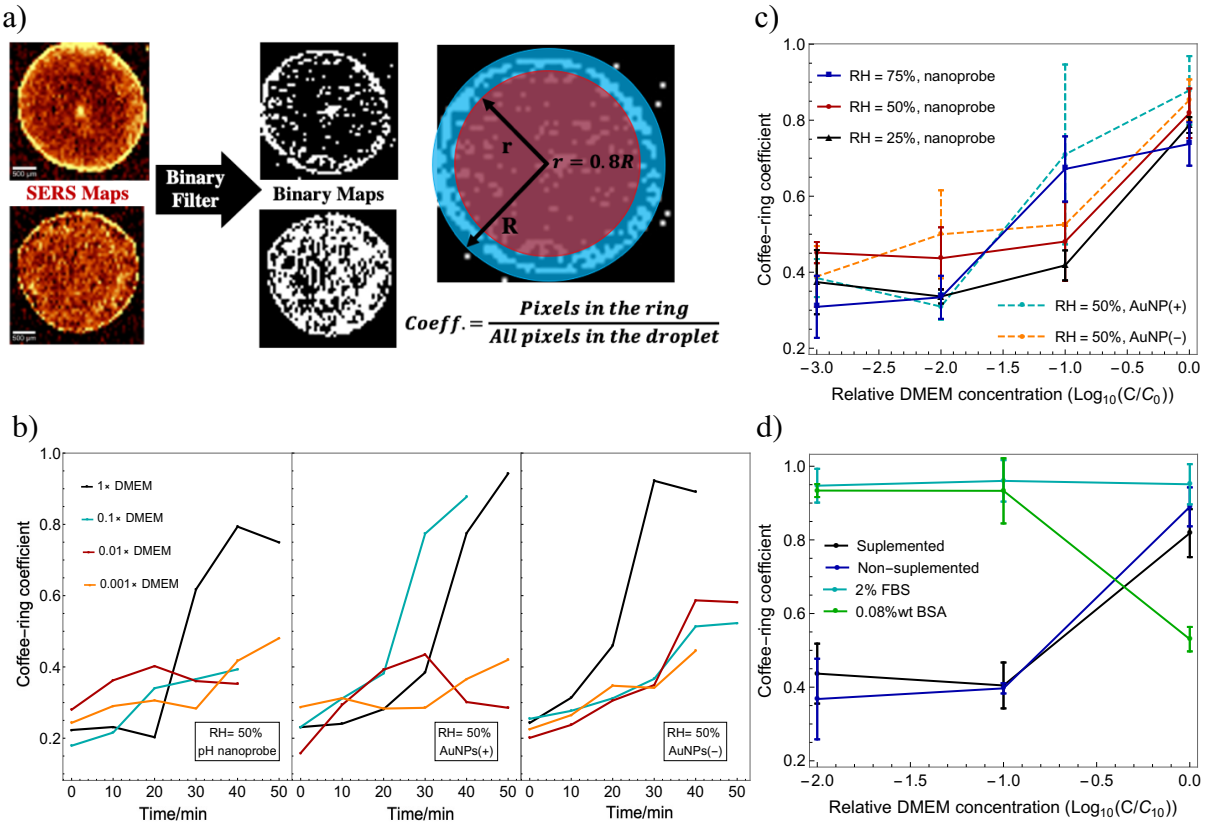


*Figure 3. a) Determination of coffee-ring coefficient (CRC). b) The final CRC (30 mins for 25% RH, 50 mins for 50% RH, and 120 mins for 75% RH) calculated for each droplet at different conditions. $C_0$ in the x-axis refers to the composition of stock DMEM (1×, Table S2). c) CRC values for different AuNPs at 50% RH as a function of time and initial DMEM concentration. d) CRC values of different droplet residues and different DMEM concentration at 50% RH, the CRC values were calculated according to the distribution of pH nanoprobe. The error bar in panel c) and d) represent the stranded deviation from duplicate measurements.*

**The correlation between the coffee-ring effect and virus infectivity.** Neither droplet evaporation rate nor final pH were impacted by droplet composition; however, both viral viability and the magnitude of the coffee ring effect were affected. We therefore investigated the potential correlation between these two latter factors. We observed lower CRC values, which

329 indicate more homogeneous distributions within dried droplets, for low DMEM (≤0.01×)
330 concentration in both supplemented and non-supplemented DMEM droplets (Figure 3d). This
331 trend correlates well with the greater decrease in Phi6 infectivity observed for lower DMEM
332 concentrations (Figure 1b). Addition of 2% FBS produced readily apparent coffee-rings (CRC >
333 0.9) at all DMEM concentrations, correlating with the observed suppression of virus inactivation.
334 Droplets with 0.08% BSA exhibited a comparable CRC to FBS droplets for lower DMEM
335 concentrations (0.1× and 0.01×); however, 1× DMEM with BSA showed a decreased CRC that
336 may reflect the altered interaction between BSA and charged molecules in concentrated
337 DMEM.[61,70,71] The greater CRC for 1× DMEM-BSA droplets coincides with increased decay of
338 Phi6. To suppress salt crystallization and the coffee-ring effect, we amended DMEM with
339 0.5%wt SDS (Figure S7). SDS addition resulted in more homogeneous droplet residues and Phi6
340 was below our limit of detection (<3 $\log_{10}$ unit). This result is consistent with previous studies
341 that have shown enhanced Phi6 inactivation in the presence of SDS.[72,73] The Pearson's
342 correlation coefficient relating the calculated CRC values and virus decay for comparable
343 conditions was -0.87, thus suggesting a strong inverse correlation. This inverse correlation
344 suggests that the magnitude of the coffee-ring effect affects virus inactivation during sessile
345 droplet evaporation.
346 A very high spatial resolution SERS map acquired under 50% RH (Figure 4) indicated that while
347 the majority of AuNPs aggregated within the coffee ring that some are retained at the edges of
348 protein-salt crystal structures formed within the interior of the droplet residue. The partitioning
349 of nanoparticulate species inside a dried droplet, including Phi6, should follow a similar pattern
350 wherein the majority of the particles aggregate within the coffee ring, and the remainder
351 associate with crystal structures that form in the residue interior. Decreased DMEM


Figure 4. Overlapping high-resolution SERS and optical images of a 1× DMEM droplet residue. As shown, AuNPs primarily aggregate within the coffee ring, however, some AuNPs are retained at the edges of the protein-salt crystals found within the residue interior.

concentrations result in less apparent or unobservable crystal structures. The droplet components become more highly aggregated when the DMEM concentration and the protein concentration, (with the exception of the DMEM-BSA system), are high. Virus accumulation due to the coffee-ring effect and protein or salt crystallization impact viability[35,36] as they result in decreased environmental exposure due to the formation of a protective microenvironment.[74]

**Conclusion.**

This study has shown that processes dictating the physical deposition of enveloped viruses within drying droplets, as illustrated using AuNPs, may affect virus infectivity during evaporation and that even the potential protection provided by proteins is altered. DMEM is a

complex media with many similarities to human exhalate and thus the observed correlation between the coffee ring effect and virus inactivation is expected to apply for environmental droplets. Designs or interventions that suppress the coffee-ring effect, such as the use of porous substrates or addition of surfactants,[23,32] may decrease virus longevity – a hypothesis supported by recent studies.[12,73] An increase in temperature also suppresses the coffee-ring effect, which along with more direct effects on viral capsid and envelope stability, may explain increased viral inactivation at high temperatures.[12,75] Recently, Fedorenko et al.[76] reported longer Phi6 persistence on glass compared to that reported herein. Glass is generally more hydrophilic than polypropylene and exhibits a larger coffee-ring effect and thus enhanced Phi6 longevity is expected. Recently, surface disinfection methods using engineered surfaces and various droplet compositions have been suggested.[77,78] Our findings will aid in the design and fabrication of such surface-dictated disinfection methods and materials. Finally, the relation between colloid deposition and viral longevity is affected by numerous environmental parameters, and cannot be independently assessed based solely upon chemical composition; therefore, future studies that examine the impacts of other surfaces and droplet compositions on the coffee ring effect are required to obtain a more mechanistic understanding of virus disinfection on surfaces.

**Supporting Information:**

Additional information on experimental details, supplemental tables, figures, and SERS maps are included in the supporting information.

**Author Information:**

Corresponding Author:

**Peter J. Vikesland** – Virginia Tech, Blacksburg, Virginia, 24060, United States; Email: pvikes@vt.edu.

Authors:

**Qishen Huang** - Virginia Tech, Blacksburg, Virginia, 24060, United States

**Wei Wang** - Virginia Tech, Blacksburg, Virginia, 24060, United States

**Acknowledgements**

This research was supported by the National Science Foundation grants (CBET-1705653 and CBET-2029911). The Virginia Tech Institute for Critical Technology and Applied Science Sustainable Nanotechnology provided instruments and laboratory resources. We gratefully thank Dr. Linsey Marr for her suggestions and support throughout this study.

**References**

(1) Allen, J. G.; Marr, L. C. Recognizing and Controlling Airborne Transmission of SARS-CoV-2 in Indoor Environments. *Indoor Air* **2020**, *30* (4), 557–558. https://doi.org/10.1111/ina.12697.

(2) Prather, K. A.; Prather, K. A.; Wang, C. C.; Schooley, R. T. Reducing Transmission of SARS-CoV-2. *Science (80-. ).* **2020**, *6197*, 1–5.

(3) Wilson, N.; Corbett, S.; Tovey, E. Airborne Transmission of Covid-19. *BMJ* **2020**, *370*, m3206. https://doi.org/10.1136/bmj.m3206.

(4) Kormuth, K. A.; Lin, K.; Prussin, A. J.; Vejerano, E. P.; Tiwari, A. J.; Cox, S. S.; Myerburg, M. M.; Lakdawala, S. S.; Marr, L. C. Influenza Virus Infectivity Is Retained in Aerosols and Droplets Independent of Relative Humidity. *J. Infect. Dis.* **2018**, *218* (5), 739–747. https://doi.org/10.1093/infdis/jiy221.

(5) Fabian, P.; McDevitt, J. J.; DeHaan, W. H.; Fung, R. O. P.; Cowling, B. J.; Chan, K. H.; Leung, G. M.; Milton, D. K. Influenza Virus in Human Exhaled Breath: An Observational Study. *PLoS One* **2008**, *3* (7). https://doi.org/10.1371/journal.pone.0002691.

(6) Lindsley, W. G.; Blachere, F. M.; Beezhold, D. H.; Thewlis, R. E.; Noorbakhsh, B.; Othumpangat, S.; Goldsmith, W. T.; McMillen, C. M.; Andrew, M. E.; Burrell, C. N.; Noti, J. D. Viable Influenza A Virus in Airborne Particles Expelled during Coughs versus Exhalations. *Influenza Other Respi. Viruses* **2016**, *10* (5), 404–413. https://doi.org/10.1111/irv.12390.

(7) Yang, W.; Elankumaran, S.; Marr, L. C. Relationship between Humidity and Influenza A Viability in Droplets and Implications for Influenza's Seasonality. *PLoS One* **2012**, *7* (10). https://doi.org/10.1371/journal.pone.0046789.

(8) Zhang, R.; Li, Y.; Zhang, A. L.; Wang, Y.; Molina, M. J. Identifying Airborne Transmission as the Dominant Route for the Spread of COVID-19. *Proc. Natl. Acad. Sci. U. S. A.* **2020**, *117* (26), 14857–14863. https://doi.org/10.1073/pnas.2009637117.

(9) Zhao, P.; Li, Y. Modeling and Experimental Validation of Microbial Transfer via Surface Touch. *Environ. Sci. Technol.* **2020**. https://doi.org/10.1021/acs.est.0c04678.

(10) Bedrosian, N.; Mitchell, E.; Rohm, E.; Rothe, M.; Kelly, C.; String, G.; Lantagne, D. A Systematic Review of Surface Contamination, Stability, and Disinfection Data on SARS-

CoV-2 (through July 10, 2020). *Environ. Sci. Technol.* **2020**, *2*. https://doi.org/10.1021/acs.est.0c05651.

(11) De Wit, E.; Van Doremalen, N.; Falzarano, D.; Munster, V. J. SARS and MERS: Recent Insights into Emerging Coronaviruses. *Nature Reviews Microbiology*. 2016, pp 523–534. https://doi.org/10.1038/nrmicro.2016.81.

(12) van Doremalen, N.; Bushmaker, T.; Morris, D. H.; Holbrook, M. G.; Gamble, A.; Williamson, B. N.; Tamin, A.; Harcourt, J. L.; Thornburg, N. J.; Gerber, S. I.; Lloyd-Smith, J. O.; de Wit, E.; Munster, V. J. Aerosol and Surface Stability of SARS-CoV-2 as Compared with SARS-CoV-1. *N. Engl. J. Med.* **2020**, *382* (16), 1564–1567. https://doi.org/10.1056/nejmc2004973.

(13) Pitol, A. K.; Julian, T. R. Community Transmission of SARS-CoV-2 by Fomites: Risks and Risk Reduction Strategies. *Environ. Sci. Technol. Lett.* **2021**. https://doi.org/10.1021/acs.estlett.0c00966.

(14) Houspie, L.; De Coster, S.; Keyaerts, E.; Narongsack, P.; De Roy, R.; Talboom, I.; Sisk, M.; Maes, P.; Verbeeck, J.; Van Ranst, M. Exhaled Breath Condensate Sampling Is Not a New Method for Detection of Respiratory Viruses. *Virol. J.* **2011**, *8*, 1–7. https://doi.org/10.1186/1743-422X-8-98.

(15) Leung, N. H. L.; Chu, D. K. W.; Shiu, E. Y. C.; Chan, K. H.; McDevitt, J. J.; Hau, B. J. P.; Yen, H. L.; Li, Y.; Ip, D. K. M.; Peiris, J. S. M.; Seto, W. H.; Leung, G. M.; Milton, D. K.; Cowling, B. J. Respiratory Virus Shedding in Exhaled Breath and Efficacy of Face Masks. *Nat. Med.* **2020**, *26* (5), 676–680. https://doi.org/10.1038/s41591-020-0843-2.

(16) Kumar, A.; Terakosolphan, W.; Hassoun, M.; Vandera, K. K.; Novicky, A.; Harvey, R.; Royall, P. G.; Bicer, E. M.; Eriksson, J.; Edwards, K.; Valkenborg, D.; Nelissen, I.; Hassall, D.; Mudway, I. S.; Forbes, B. A Biocompatible Synthetic Lung Fluid Based on Human Respiratory Tract Lining Fluid Composition. *Pharm. Res.* **2017**, *34* (12), 2454–2465. https://doi.org/10.1007/s11095-017-2169-4.

(17) Riddell, S.; Goldie, S.; Hill, A.; Eagles, D.; Drew, T. W. The Effect of Temperature on Persistence of SARS-CoV-2 on Common Surfaces. *Virol. J.* **2020**, *17* (1), 1–7. https://doi.org/10.1186/s12985-020-01418-7.

(18) Chin, A. W. H.; Chu, J. T. S.; Perera, M. R. A.; Hui, K. P. Y.; Yen, H.-L.; Chan, M. C. W.; Peiris, M.; Poon, L. L. M. Stability of SARS-CoV-2 in Different Environmental Conditions. *The Lancet Microbe* **2020**, *1* (1), e10. https://doi.org/10.1016/s2666-5247(20)30003-3.

(19) Biryukov, J.; Boydston, J. A.; Dunning, R. A.; Yeager, J. J.; Wood, S.; Reese, A. L.; Ferris, A.; Miller, D.; Weaver, W.; Zeitouni, N. E.; Phillips, A.; Freeburger, D.; Hooper, I.; Ratnesar-Shumate, S.; Yolitz, J.; Krause, M.; Williams, G.; Dawson, D. G.; Herzog, A.; Dabisch, P.; Wahl, V.; Hevey, M. C.; Altamura, L. A. Increasing Temperature and Relative Humidity Accelerates Inactivation of SARS-CoV-2 on Surfaces. *mSphere* **2020**, *5* (4). https://doi.org/10.1128/msphere.00441-20.

(20) Morris, D. H.; Yinda, K. C.; Gamble, A.; Rossine, F. W.; Huang, Q.; Bushmaker, T.; Fischer, R. J.; Jeremiah Matson, M.; van Doremalen, N.; Vikesland, P. J.; Marr, L. C.; Munster, V. J.; Lloyd-Smith, J. O. Mechanistic Theory Predicts the Effects of Temperature and Humidity on Inactivation of Sars-Cov-2 and Other Enveloped Viruses. *Elife* **2021**, *10*. https://doi.org/10.7554/ELIFE.65902.

(21) Whitworth, C.; Mu, Y.; Houston, H.; Martinez-Smith, M.; Noble-Wang, J.; Coulliette-

Salmond, A.; Rose, L. Persistence of Bacteriophage Phi 6 on Porous and Nonporous Surfaces and the Potential for Its Use as an Ebola Virus or Coronavirus Surrogate. *Appl. Environ. Microbiol.* **2020**, *86* (17). https://doi.org/10.1128/AEM.01482-20.

(22) Aboubakr, H. A.; Sharafeldin, T. A.; Goyal, S. M. Stability of SARS-CoV-2 and Other Coronaviruses in the Environment and on Common Touch Surfaces and the Influence of Climatic Conditions: A Review. *Transboundary and Emerging Diseases*. Blackwell Publishing Ltd 2020. https://doi.org/10.1111/tbed.13707.

(23) Mampallil, D.; Eral, H. B. A Review on Suppression and Utilization of the Coffee-Ring Effect. *Adv. Colloid Interface Sci.* **2018**, *252*, 38–54. https://doi.org/10.1016/j.cis.2017.12.008.

(24) Deegan, R. D.; Bakajin, O.; Dupont, T. F.; Huber, G.; Nagel, S. R.; Witten, T. A. Capillary Flow as the Cause of Ring Stains from Dried Liquid Drops. *Nature* **1997**, *389* (23), 827–829.

(25) Sempels, W.; De Dier, R.; Mizuno, H.; Hofkens, J.; Vermant, J. Auto-Production of Biosurfactants Reverses the Coffee Ring Effect in a Bacterial System. *Nat. Commun.* **2013**, *4*, 1–8. https://doi.org/10.1038/ncomms2746.

(26) Ren, J.; Crivoi, A.; Duan, F. Disk-Ring Deposition in Drying a Sessile Nano Fluid Droplet with Enhanced Marangoni Effect and Particle Surface Adsorption. *Langmuir* **2020**. https://doi.org/10.1021/acs.langmuir.0c02607.

(27) Zhong, X.; Duan, F. Flow Regime and Deposition Pattern of Evaporating Binary Mixture Droplet Suspended with Particles. *Eur. Phys. J. E* **2016**, *39* (2), 1–6. https://doi.org/10.1140/epje/i2016-16018-5.

(28) Katre, P.; Balusamy, S.; Banerjee, S.; Chandrala, L. D.; Sahu, K. C. Evaporation Dynamics of a Sessile Droplet of Binary Mixture Laden with Nanoparticles. *Langmuir* **2021**, *37*, 6311–6321. https://doi.org/10.1021/acs.langmuir.1c00806.

(29) Chen, L.; Evans, J. R. G. Drying of Colloidal Droplets on Superhydrophobic Surfaces. *J. Colloid Interface Sci.* **2010**, *351* (1), 283–287. https://doi.org/10.1016/j.jcis.2010.07.037.

(30) Bhardwaj, R.; Fang, X.; Somasundaran, P.; Attinger, D. Self-Assembly of Colloidal Particles from Evaporating Droplets: Role of DLVO Interactions and Proposition of a Phase Diagram. *Langmuir* **2010**, *26* (11), 7833–7842. https://doi.org/10.1021/la9047227.

(31) Morales, V. L.; Parlange, J. Y.; Wu, M.; Pérez-Reche, F. J.; Zhang, W.; Sang, W.; Steenhuis, T. S. Surfactant-Mediated Control of Colloid Pattern Assembly and Attachment Strength in Evaporating Droplets. *Langmuir* **2013**, *29* (6), 1831–1840. https://doi.org/10.1021/la304685b.

(32) Yunker, P. J.; Still, T.; Lohr, M. A.; Yodh, A. G. Suppression of the Coffee-Ring Effect by Shape-Dependent Capillary Interactions. *Nature* **2011**, *476* (7360), 308–311. https://doi.org/10.1038/nature10344.

(33) Zhou, W.; Hu, A.; Bai, S.; Ma, Y.; Su, Q. Surface-Enhanced Raman Spectra of Medicines with Large-Scale Self-Assembled Silver Nanoparticle Films Based on the Modified Coffee Ring Effect. *Nanoscale Res. Lett.* **2014**, *9* (1), 1–9. https://doi.org/10.1186/1556-276X-9-87.

(34) Wang, W.; Yin, Y.; Tan, Z.; Liu, J. Coffee-Ring Effect-Based Simultaneous SERS Substrate Fabrication and Analyte Enrichment for Trace Analysis. *Nanoscale* **2014**, *6* (16),

9588–9593. https://doi.org/10.1039/c4nr03198a.

(35) Hoff, J. C.; Akin, E. W. *Microbial Resistance to Disinfectants: Mechanisms and Significance*; 1986; Vol. 69.

(36) Gerba, C. P.; Betancourt, W. Q. Viral Aggregation: Impact on Virus Behavior in the Environment. *Environ. Sci. Technol.* **2017**, *51* (13), 7318–7325. https://doi.org/10.1021/acs.est.6b05835.

(37) Prussin, A. J.; Schwake, D. O.; Lin, K.; Gallagher, D. L.; Buttling, L.; Marr, L. C. *Survival of the Enveloped Virus Phi6 in Droplets as a Function of Relative Humidity, Absolute Humidity, and Temperature*; 2018; Vol. 84. https://doi.org/10.1128/AEM.00551-18.

(38) Lin, K.; Marr, L. C. Humidity-Dependent Decay of Viruses, but Not Bacteria, in Aerosols and Droplets Follows Disinfection Kinetics. *Environ. Sci. Technol.* **2020**, *54* (2), 1024–1032. https://doi.org/10.1021/acs.est.9b04959.

(39) Lahr, R. H.; Vikesland, P. J. Surface-Enhanced Raman Spectroscopy (SERS) Cellular Imaging of Intracellulary Biosynthesized Gold Nanoparticles. *ACS Sustain. Chem. Eng.* **2014**, *2* (7), 1599–1608. https://doi.org/10.1021/sc500105n.

(40) Wei, H.; Vejerano, E. P.; Leng, W.; Huang, Q.; Willner, M. R.; Marr, L. C.; Vikesland, P. J. Aerosol Microdroplets Exhibit a Stable PH Gradient. *Proc. Natl. Acad. Sci.* **2018**, *115* (28), 7272–7277. https://doi.org/10.1073/pnas.1720488115.

(41) Rasheed, A.; Sharma, S.; Kabi, P.; Saha, A.; Chaudhuri, S.; Basu, S. Precipitation Dynamics of Surrogate Respiratory Sessile Droplets Leading to Possible Fomites. *J. Colloid Interface Sci.* **2021**, *600*, 1–13. https://doi.org/10.1016/j.jcis.2021.04.128.

(42) Bhattacharjee, S.; Ryan, J. N.; Elimelech, M. Virus Transport in Physically and Geochemically Heterogeneous Subsurface Porous Media. *J. Contam. Hydrol.* **2002**, *57* (3–4), 161–187. https://doi.org/10.1016/S0169-7722(02)00007-4.

(43) Sasidharan, S.; Torkzaban, S.; Bradford, S. A.; Cook, P. G.; Gupta, V. V. S. R. Temperature Dependency of Virus and Nanoparticle Transport and Retention in Saturated Porous Media. *J. Contam. Hydrol.* **2017**, *196*, 10–20. https://doi.org/10.1016/j.jconhyd.2016.11.004.

(44) Li, Z.; Miao, X.; Xing, K.; Zhu, A.; Ling, L. Enhanced Electrochemical Recognition of Double-Stranded DNA by Using Hybridization Chain Reaction and Positively Charged Gold Nanoparticles. *Biosens. Bioelectron.* **2015**, *74*, 687–690. https://doi.org/10.1016/j.bios.2015.06.070.

(45) Yuan, H.; Khoury, C. G.; Hwang, H.; Wilson, C. M.; Grant, G. A.; Vo-Dinh, T. Gold Nanostars: Surfactant-Free Synthesis, 3D Modelling, and Two-Photon Photoluminescence Imaging. *Nanotechnology* **2012**, *23* (7). https://doi.org/10.1088/0957-4484/23/7/075102.

(46) Wei, H.; Willner, M. R.; Marr, L. C.; Vikesland, P. J. Highly Stable SERS PH Nanoprobes Produced by Co-Solvent Controlled AuNP Aggregation. *Analyst* **2016**, *141* (17), 5159–5169. https://doi.org/10.1039/c6an00650g.

(47) Leng, W.; Pati, P.; Vikesland, P. J. Room Temperature Seed Mediated Growth of Gold Nanoparticles: Mechanistic Investigations and Life Cycle Assesment. *Environ. Sci. Nano* **2015**, *2* (5), 440–453. https://doi.org/10.1039/C5EN00026B.

(48) Hu, H.; Larson, R. G. Evaporation of a Sessile Droplet on a Substrate. *J. Phys. Chem. B* **2002**, *106* (6), 1334–1344. https://doi.org/10.1021/jp0118322.

(49) Hwang, I. G.; Kim, J. Y.; Weon, B. M. Droplet Evaporation with Complexity of

Evaporation Modes. *Appl. Phys. Lett.* **2017**, *110* (3), 31602. https://doi.org/10.1063/1.4974292.

(50) Wei, H.; Leng, W.; Song, J.; Willner, M. R.; Marr, L. C.; Zhou, W.; Vikesland, P. J. Improved Quantitative SERS Enabled by Surface Plasmon Enhanced Elastic Light Scattering. *Anal. Chem.* **2018**, *90* (5), 3227–3237. https://doi.org/10.1021/acs.analchem.7b04667.

(51) Morris, D. H.; Yinda, K. C.; Gamble, A.; Rossine, F. W.; Huang, Q.; Bushmaker, T.; Fischer, R. J.; Matson, M. J.; van Doremalen, N.; Vikesland, P. J.; Marr, L. C.; Munster, V. J.; Lloyd-Smith, J. O. The Effect of Temperature and Humidity on the Stability of SARS-CoV-2 and Other Enveloped Viruses. *bioRxiv Prepr. Serv. Biol.* **2020**. https://doi.org/10.1101/2020.10.16.341883.

(52) Marr, L. C.; Tang, J. W.; Van Mullekom, J.; Lakdawala, S. S. Mechanistic Insights into the Effect of Humidity on Airborne Influenza Virus Survival, Transmission and Incidence. *J. R. Soc. Interface* **2019**, *16* (150). https://doi.org/10.1098/rsif.2018.0298.

(53) Zhong, X.; Crivoi, A.; Duan, F. Sessile Nanofluid Droplet Drying. *Adv. Colloid Interface Sci.* **2015**, *217*, 13–30. https://doi.org/10.1016/j.cis.2014.12.003.

(54) Kovalchuk, N. M.; Trybala, A.; Starov, V. M. Evaporation of Sessile Droplets. *Current Opinion in Colloid and Interface Science*. Elsevier Ltd August 1, 2014, pp 336–342. https://doi.org/10.1016/j.cocis.2014.07.005.

(55) Soulié, V.; Karpitschka, S.; Lequien, F.; Prené, P.; Zemb, T.; Moehwald, H.; Riegler, H. The Evaporation Behavior of Sessile Droplets from Aqueous Saline Solutions. *Phys. Chem. Chem. Phys.* **2015**, *17* (34), 22296–22303. https://doi.org/10.1039/c5cp02444g.

(56) Chatterjee, S.; Kumar, M.; Murallidharan, J. S.; Bhardwaj, R. Evaporation of Initially Heated Sessile Droplets and the Resultant Dried Colloidal Deposits on Substrates Held at Ambient Temperature. *Langmuir* **2020**, *36* (29), 8407–8421. https://doi.org/10.1021/acs.langmuir.0c00756.

(57) Gorr, H. M.; Zueger, J. M.; McAdams, D. R.; Barnard, J. A. Salt-Induced Pattern Formation in Evaporating Droplets of Lysozyme Solutions. *Colloids Surfaces B Biointerfaces* **2013**, *103*, 59–66. https://doi.org/10.1016/j.colsurfb.2012.09.043.

(58) Sefiane, K. Patterns from Drying Drops. *Advances in Colloid and Interface Science*. Elsevier B.V. 2014, pp 372–381. https://doi.org/10.1016/j.cis.2013.05.002.

(59) Yang, W.; Marr, L. C. Mechanisms by Which Ambient Humidity May Affect Viruses in Aerosols. *Appl. Environ. Microbiol.* **2012**, *78* (19), 6781–6788. https://doi.org/10.1128/AEM.01658-12.

(60) Huang, Qishen; Wei, Haoran;Marr, Linsey C.; Vikesland, P. J.; Huang, Qishen; Wei, Haora,; Vikesland, P. J. Direct Quantification of the Effect of Ammonium on Aerosol Droplet PH. *Environ. Sci. Technol. (Under Rev.* **2020**. https://doi.org/10.1021/acs.est.0c07394.

(61) Mayarani, M.; Basavaraj, M. G.; Satapathy, D. K. Viscoelastic Particle-Laden Interface Inhibits Coffee-Ring Formation. *Langmuir* **2018**, *34* (47), 14294–14301. https://doi.org/10.1021/acs.langmuir.8b02739.

(62) Andrew, C. K.; Darst, S. A.; Kornberg, R. D.; Robertson, C. R.; Gast, A. P. *Dendritic Growth of Two-Dimensional Protein Crystals*; 1992; Vol. 8.

https://doi.org/10.1021/la00046a003.

(63) Dutta Choudhury, M.; Dutta, T.; Tarafdar, S. Growth Kinetics of NaCl Crystals in a Drying Drop of Gelatin: Transition from Faceted to Dendritic Growth. *Soft Matter* **2015**, *11* (35), 6938–6947. https://doi.org/10.1039/c5sm00742a.

(64) Hegde, O.; Chatterjee, R.; Rasheed, A.; Chakravortty, D.; Basu, S. Vapor Mediation as a Tool to Control Micro-Nano Scale Dendritic Crystallization and Preferential Bacterial Distribution in Drying Respiratory Droplets. *bioRxiv* **2021**, 2021.06.18.448992. https://doi.org/10.1101/2021.06.18.448992.

(65) Choudhury, M. D.; Dutta, S.; Tarafdar, S. Pattern Formation in Droplets of Starch Gels Containing NaCl Dried on Different Surfaces. *Colloids and Surfaces A: Physiochemical an Engineering Aspects* **2013**, *432*, 110--118. https://doi.org/10.1016/j.colsurfa.2013.04.064

(66) Pathak, B.; Hatte, S.; Basu, S. Evaporation Dynamics of Mixed-Nanocolloidal Sessile Droplets. *Langmuir* **2017**, *33* (49), 14123–14129. https://doi.org/10.1021/acs.langmuir.7b03578.

(67) Malla, L. K.; Bhardwaj, R.; Neild, A. Analysis of Profile and Morphology of Colloidal Deposits Obtained from Evaporating Sessile Droplets. *Colloids Surfaces A Physicochem. Eng. Asp.* **2019**, *567*, 150–160. https://doi.org/10.1016/j.colsurfa.2019.01.028.

(68) Zhou, L.; Yang, Y.; Du, X.; Yang, Y. Effect of Sessile Binary Droplet Evaporation at Different Ambient Temperatures on Interfacial Profile near the Triple Line. *Exp. Therm. Fluid Sci.* **2019**, *103*, 108–117. https://doi.org/10.1016/j.expthermflusci.2018.12.034.

(69) Huang, C.; Wang, J.; Lv, X.; Liu, L.; Liang, L.; Hu, W.; Luo, C.; Wang, F.; Yuan, Q. Redefining Molecular Amphipathicity in Reversing the "Coffee-Ring Effect": Implications for Single Base Mutation Detection. *Langmuir* **2018**, *34* (23), 6777–6783. https://doi.org/10.1021/acs.langmuir.8b01248.

(70) Jeyachandran, Y. L.; Mielczarski, E.; Rai, B.; Mielczarski, J. A. Quantitative and Qualitative Evaluation of Adsorption/Desorption of Bovine Serum Albumin on Hydrophilic and Hydrophobic Surfaces. *Langmuir* **2009**, *25* (19), 11614–11620. https://doi.org/10.1021/la901453a.

(71) Devineau, S.; Anyfantakis, M.; Marichal, L.; Kiger, L.; Morel, M.; Rudiuk, S.; Baigl, D. Protein Adsorption and Reorganization on Nanoparticles Probed by the Coffee-Ring Effect: Application to Single Point Mutation Detection. *J. Am. Chem. Soc.* **2016**, *138* (36), 11623–11632. https://doi.org/10.1021/jacs.6b04833.

(72) Chattopadhyay, D.; Chattopadhyay, S.; Lyon, W. G.; Wilson, J. T. Effect of Surfactants on the Survival and Sorption of Viruses. *Environ. Sci. Technol.* **2002**, *36* (19), 4017–4024. https://doi.org/10.1021/es0114097.

(73) Lin, K.; Schulte, C. R.; Marr, L. C. Survival of MS2 and Φ6 Viruses in Droplets as a Function of Relative Humidity, PH, and Salt, Protein, and Surfactant Concentrations. *PLoS One* **2020**, *15* (12 December). https://doi.org/10.1371/journal.pone.0243505.

(74) Martínez Vimbert, R.; M, A. L.; D, C. S.; J, G. R.; P, M. A.; Vimbert, M. R.; Loyo, A. M.; Sánchez, C. D.; Raurich, G. J.; Asensio, M. P. Evidence of OH · Radicals Disinfecting Indoor Air and Surfaces in a Harmless for Humans Method. *Int. J. Eng. Res. Sci.* **2020**, *6* (4), 26–38.

(75) Li, Y.; Yang, Q.; Li, M.; Song, Y. Rate-Dependent Interface Capture beyond the Coffee-

Ring Effect. *Sci. Rep.* **2016**, *6* (April), 1–8. https://doi.org/10.1038/srep24628.

(76) Fedorenko, A.; Grinberg, M.; Orevi, T.; Kashtan, N. Virus Survival in Evaporated Saliva Microdroplets Deposited on Inanimate Surfaces. *bioRxiv* **2020**. https://doi.org/10.1101/2020.06.15.152983.

(77) Behzadinasab, S.; Chin, A.; Hosseini, M.; Poon, L.; Ducker, W. A. A Surface Coating That Rapidly Inactivates SARS-CoV-2. *ACS Appl. Mater. Interfaces* **2020**, *12* (31), 34723–34727. https://doi.org/10.1021/acsami.0c11425.

(78) Talebian, S.; Wallace, G. G.; Schroeder, A.; Stellacci, F.; Conde, J. Nanotechnology-Based Disinfectants and Sensors for SARS-CoV-2. *Nat. Nanotechnol.* **2020**, *15* (8), 618–621. https://doi.org/10.1038/s41565-020-0751-0.

## TOC Graphic